IV. Pattern Recognition and Particle Identification

Introduction

This is not the first neutrino experiment to use imaging water Cherenkov detectors. The data reduction and analysis methods originally developed by the Kamiokande and IMB detectors serve as an invaluable basis for the techniques to be used in E889. They are described in detail in Ph.D. theses cited at the end of this chapter. Accordingly, we do not here attempt an in-depth discussion of those relatively well-known methods. Instead, we discuss their application to the needs of E889 to show that those needs can be well satisfied. Specifically, we address the important questions of muon-electron separation; of the efficiency with which WNC(π^0) events can be recognized and also distinguished from WCC(π^0) events; and the extent to which aberrant WNC(π^0) events might constitute a background in the $\nu_\mu \leftrightarrow \nu_e$ search. With the neutrino beam for E889 described in Chapter III, the dominant neutrino reaction product is a quasielastic muon, and to a much lesser extent a quasielastic electron, both single Cherenkov ring events. Single pion production, yielding two- or three-ring events is also an important event type. In addition, we comment briefly on our progress in developing methods of automatic pattern recognition and reconstruction of multiring events.

Previously Developed Methods of Analysis

Neutrinos interacting in a large water detector will produce charged particles, each of which may produce a Cherenkov cone of ultraviolet and visible photons. Where the cone intersects the inner surface of the detector tank a ring-like pattern of PMT will be lit. A pattern may consist of a single ring, two or more separated or overlapping rings, or in a few cases PMT hits with no clear organization. The recorded time, amplitude and known location of each hit PMT provide all the information necessary to reconstruct the event and classify it according to the number and quality of rings observed. Both the disappearance and appearance modes of E889 depend on the efficient classification of hit patterns, specifically, discrimination among the patterns produced by muon, electron, and weak neutral current (WNC(π^0)) events, and weak charged current (WCC(π^0)) events. Previous underground experiments performed this task by reconstructing the vertex and particle direction corresponding to each designated ring, supplemented by visual scanning of the events. Reconstruction of single ring events was done automatically, i.e., without direct human operator intervention, while multiring events were reconstructed with an interactive manual program.

The resolution in position of event vertices, σ_{pos}, and of track directions, σ_θ, for single ring muon and electron events is well understood in both the Kamiokande and IMB detectors. σ_{pos} as a function of the number of photoelectrons (and momentum) is shown in Fig. 1a; σ_θ in Fig. 1b. These results obtained with Monte Carlo generated events are from the thesis of M. Takita. Essentially the same results are presented in the theses of D.W. Casper and E.D. Frank, all cited here. For E889 we expect somewhat better position resolutions due to the better quality of time information from our 20 cm PMTs than the Kamioka PMTs. Our present simulations suggest that position resolution of $\sim$ 30 cm parallel and $\sim$ 15 cm perpendicular to the direction of a particle of 1 GeV/c is possible. This is entirely adequate for the experiment. The energy response of the detector for various particles is shown in Figure V.6.

E889 Analysis

The same procedures will be followed in analyzing the data of E889 which, like Kamiokande and IMB, is basically an electronic detector. From the times recorded by the hit PMT, a first estimate of the vertex of a given event is made. This is iterated after correcting the raw times for the flight path of the Cherenkov light from the estimated vertex to a given PMT. For a single ring the corrected times fall within an interval of less than 20 ns FWHM, superimposed on a flat distribution due to scattered Cherenkov light and multiple scattering of delta rays. Another iteration in which much of the flat distribution is not included in the vertex calculation usually brings the FWHM value of corrected time distribution to less than 15 ns. There are several refinements to this procedure, e.g., introducing the charge amplitude of the hits independently of or in combination with the time information, limiting the analysis to events with a minimum number of hit PMT and charge, etc. Using the final iterated vertex coordinates and the known positions of the hit PMT, the direction of the axis of the Cherenkov cone, i.e., the particle direction, can be found and specified by its direction cosines. The corrected total charge observed in the ring yields the particle momentum which can be checked against its range from properties of the ring.

With the vertex specified the events within the fiducial volume can be selected. The quality of these events, signified by the errors in the vertex coordinates and track direction cosines, the width of the time distribution, the ratio of the number of tightly bunched-in-time PMT hits to the number in the flat time distribution, etc, is used to determine whether the event under consideration is a single-ring event or not. In E889 we expect roughly 20% of

events to involve more than one ring, so that this procedure separates the dominant single ring quasielastic muon sample, with each event fully reconstructed, from the multiring sample, which requires further analysis.

It should be emphasized that the method of analysis outlined here which provides first order pattern recognition is the result purely of computer processing of PMT signals. No visual scanning of events is necessary, apart from the initial checks on the validity of the programs and the parameters. It involves an analysis simpler in form and less demanding of computer time than analyses of magnetic field-chamber-counter experiments.

The roughly 20% of the data that does not satisfy the single ring criteria needs separate analysis. This can be done for the number of events of that type expected in E889 by an operator assisted interactive program which handles each ring in a multiring event, i.e., identifies the PMT hits belonging to each ring and reconstructs the parameters of each ring separately, and of the complete event in combination. Event samples consisting of 10^4 events in D1 would contain about 2×10^3 multiring events to be analyzed in this way, not a serious burden for the collaboration since only analysis of large samples in D1 and D3 is required to set the criteria and conditions for the analyses of all the multiring events in D24 and D68.

It is, however, an interesting and challenging problem to develop programs capable of automatic pattern recognition and reconstruction of multiring events. While not required to do the experiment, these would facilitate data analysis and provide useful redundancy. We have begun work in this direction which is briefly described in the last section of this chapter.

Muon-Electron Separation

There are available a number of algorithms with which to distinguish single-rings produced by muons (or charged pions) from those produced by electrons. These are described in detail and evaluated in the references given here. Muon-electron separation has been accomplished previously with high efficiency, as indicated by the agreement between the results from the IMB and Kamiokande collaborations on atmospheric neutrinos, and by the internal consistency of the results obtained within each collaboration when identical event samples are processed using different algorithms. Again, this aspect of the analysis is carried out at least in first order by computer processing. The small number of electron (single showering ring) events expected in E889 permits them to be studied visually as well as electronically without appreciable extra effort. Recently, a 1-kiloton test imaging water Cherenkov detector has been exposed to muon and electron beams at KEK of several momenta, differently positioned

within the detector. Some unpublished results—confirming in quantitative detail the previously claimed muon-electron separation—are shown in Fig. 2. One sees that the degree of muon-electron separation depends on particle momentum, but by 400 MeV/c the separation achieved with the algorithms employed in the analysis is complete within the statistical limits of the samples. These preliminary results will soon be supplemented by larger event samples.

The particle identification requirement in E889, where the relative intensities of electron and muon are in the approximate ratio 10^{-2}, is moderately severe. Misidentification of muons from $\nu_\mu n \to \mu^- p$ as if they were electrons coming from $\nu_e \mu \to e^- p$ should be less than 1 part in 10^3, if the search for oscillations in the appearance channel $\nu_\mu \leftrightarrow \nu_e$ is to be carried out below the 1% level. We are confident that this can be accomplished in part because of the data in Fig. 2. Also, by combining several algorithms each known to be of $\gtrsim$ 90% efficiency, and each based on an independent quantity, e.g., PMT hit location, PMT hit time, PMT hit charge, with visual scanning of the small number of electron candidates, there appears to be no intractable difficulty in reaching 1 part in 10^3.

Note that exclusion of questionable events from both the muon and electron samples will not induce an apparent positive oscillation effect, but dilution of a real $\nu_\mu \leftrightarrow \nu_e$ signal must be guarded against. Note further that muon and electron event selection criteria will be set empirically by study of those event types in the upstream detectors D1 and D3, where the electron to muon number ratio to be expected in the far detectors in the absence of oscillations will also be measured. Muon-electron discrimination is discussed again briefly in the section on event recognition below.

Multiring Events

The other ring patterns of interest are the products of exclusive channel inelastic reactions, principally those involving single pion production, i.e., the flavor preserving WNC(π^0) reactions $\nu_n \to \nu n \pi^0$ and $\nu p \to \nu p \pi^0$, the single WCC(π^0) reaction $\nu_\mu n \to \mu^- p \pi^0$, and the WCC($\pi^\pm$) reactions. The patterns of all these reactions are in general distinguished by the presence of two or more rings. Given the rates of these reactions with respect to the quasielastic reaction rate, discussed earlier in Chapter II and later in Chapter V, the problem of identification is focused on distinguishing the relatively few events with more than a single ring from the multitude with only a single ring. The inverse problem is relatively unimportant. With the usual automatic pattern recognition and reconstruction of single ring events described above, those events in the detector fiducial volume not satisfying an event-quality

criterion, e.g., a chi-square fit to the ring, can efficiently be set aside for visual inspection and interactive manual reconstruction. All of the data in D24 and D68 can be handled in this way, and large data samples from D1 and D3 treated the same way to fix event selection criteria and serve the purpose of normalization. The efficiency with which visual scanning permits discrimination of WNC(π^0) events from WCC(π^0) is treated in the next section, as is the discrimination of WNC(π^0) from electrons when one of the rings from the π^0 is not evident.

Visual Event Recognition

Simulated QE(μ), QE(e), WCC(π^0), and WNC(π^0) events have been generated and scanned visually. In all cases, the particles were generated by allowing the spectra of ν_μ and ν_e planned for E889 to interact in a cylinder of water 15m high $\times$ 15m in diameter. The PMT lining the walls of the cylinder were simulated by sensitive disks 25.2 cm in diameter, an approximation to physical PMT 20 cm in diameter with Winston cone light collectors. The spectral response of the PMT was included in the simulation. 2195 such tubes are placed uniformly on the inner walls of the detector tank to attain 10.3% coverage. This configuration allows efficient visual identification of all WNC and WCC events for a relatively small total area of photocathode. It is possible that a non-uniform configuration of PMT would be more efficient in light collection for E889, but this has not yet been studied with sufficient care.

Quasielastic muon events have single Cherenkov rings with sharp outer edges and relatively few PMT hits outside the ring. Quasielastic electron events have single rings with fuzzy edges and many hits outside the ring due to multiple scattering and bremsstrahlung. Examples of real and simulated muon and electron events from the Kamiokande detector illustrating these properties are shown in Figs. 15 and 16 of Chapter II. Similar displays of Monte Carlo muon and electron events using E889 programs are shown in Chapter V. When quantified, the event properties in those figures form the bases of the algorithms for muon-electron identification mentioned above.

Most WNC(π^0) events display two fuzzy edged rings; most WCC(π^0) events exhibit a clear muon ring in addition. Examples of a WNC(π^0) event and a WCC(π^0) event from the E889 Monte Carlo event simulation and display programs are shown in Figs. 3 and 4, which exhibit the characteristic properties of those event types.

In our visual scanning exercise of π^0 events, positive event type recognition is considered to be achieved when the correct number and type of rings are clearly observed. However,

interaction kinematics and detector response may lead some events to have signatures which are less than ideal. For example, asymmetric (π^0) decays may produce a gamma ray whose shower has too little energy to yield a clear ring, causing only one ring to be observed. Similarly, if the vertex of the reaction is near the boundary of the fiducial volume, one of the gammas from a symmetric decay may not convert far enough within the fiducial volume to produce a clear ring, or indeed any ring. Alternatively, $\pi^0$with higher momentum will yield gamma rays with overlapping rings, which in some cases appear as a single ring. Conversely, a small fraction of WNC(π^0) events may show three fuzzy edged rings if either the π^0decay is directly to γe^+e^- or if one of the e^+e^- pair produced in the gamma conversion scatters at a large angle.

For these reasons the results of a visual scan of one thousand WNC(π^0) and one thousand WCC(π^0) events, shown in Table 1, are divided into the following categories: one ring; one ring plus a number of PMT hits representing a substantial part of, but not a complete, second ring; two rings; two rings plus; three rings; three rings plus; and unidentifiable events. In addition, the WCC(π^0) events have been divided into those in which a muon ring is clearly identified, and those in which the muon is not evident. The fiducial volume for the two samples is a cylinder of diameter 13 m and height 13 m. Events with fewer than 50 PMT hits or fewer than 300 photoelectrons (p (π^0) $\sim 10^2$ MeV/c) were not included.

Combining the results for the (1 ring +) and 2-ring samples in Table 1 yields a detection efficiency of 75% for WNC(π^0) events. If, however, the criterion for π^0identification is restricted to require 2 rings which reconstruct manually to give the invariant mass of the π^0, the detection efficiency should be approximately 50%. This exercise was originally carried out on Monte Carlo generated events by Katsushi Arisaka in the first Ph.D. thesis from Kamiokande; his result is shown in Fig. 5. The results in Table 1 have been reproduced independently by three different scans.

Comparing the data in the two WCC columns indicates that at least 81% of the WCC(π^0) events can be identified by the presence of a clear muon ring. Hence, efficient rejection of the WCC(π^0) background at the 20% level in the WNC(π^0) sample is possible simply by requiring a clear muon ring, since both WNC(π^0) and WCC(π^0) production occur at approximately 20% and 15%, respectively, of the quasielastic muon rate. The approximately 20% of 1-ring events in the top row of Table 1 are not a serious background for the $\nu_\mu \leftrightarrow \nu_e$ oscillation search as shown in Chapter V.4.

Again, note that in both the case of WCC(π^0) contamination of the WNC(π^0) signal, and the case of 1-ring π^0 contamination of the electron signal, the upstream detectors D1

and D3 are used to set empirically the criteria for event selection and to normalize the ratios of event types to be detected in the far detectors. No reliance on Monte Carlo predictions is necessary.

PMT Diameter and Areal Coverage

Similar scans of WNC and WCC(π^0) events were performed for two other PMT coverage schemes to check that the coverage adopted for E889 is adequate for those event types, which require larger coverage for efficient detection than do the single ring events.. Scheme II used 1807 PMT each 20 cm in diameter and having no light collector. The total coverage was 5.4%. Scheme III used 1002 50 cm diameter PMT also without light collectors (as in Kamiokande II) for a total coverage of 18.6%. Results for the WNC scan, along with those from scheme I (10.3% coverage), are shown in Table 2. Since the visual scans for schemes II and III did not include the categories of fractional rings, events in those categories in scheme I were evenly divided between integral ring categories for the sake of comparison.

Table 2 shows that in going from 5.4% to 10.3% coverage significantly more 2-ring events are identified. At the same time the number of WNC(π^0) 1-ring events decreases correspondingly. Going to 18.6% coverage produces no appreciable increase in the number of 2-ring events observed, indicating that an approximate plateau in coverage is reached at 10.3%. Similar results are obtained in the scan of WCC events. Even the 5.4% coverage is adequate for single ring events.

Automated Pattern Recognition and Reconstruction of Multiring Events.

There are several methods of automated pattern recognition of multiring events aimed largely at facilitating data analysis in E889, which are currently being explored. These make use of pattern properties such as the fraction of PMT hits outside the Cherenkov cone, and the circularity of the event pattern, and attempt ring recognition and reconstruction by automatic scanning and neural networks.

1. The fraction of PMT hits outside the Cherenkov cone can be found by first computing an event vertex and apparent track direction from timing information alone. The reconstructed apparent track direction is taken to be the average of all rays connecting the vertex to hit PMT locations, and the angle between each ray and the apparent track direction is computed. The fraction of hits, including random hits from light scattering,

etc., with angles in various angular regions outside the nominal Cherenkov ring may be used to discriminate between single and multiring events.

2. Circularity is a measure of the moments of the PMT hit pattern projected onto a sphere. This method utilizes the idea that momenta of the PMT charge distribution of multiring events with respect to the angular separation from the mean should be larger in one azimuthal direction than the corresponding distribution for single ring events.

3. A possible automatic ring search routine employs a faster scan to locate and identify the number of rings in a hit pattern the same way the eye does in visual scanning. This method is quite general and does not depend upon knowing the event vertex. A search for hits is made, first over the rows, then the columns of the PMT array in the detector. The first hit encountered in each row and column which is above a given photoelectron threshold is saved. The saved set of hits is thus the outline of the event pattern. When tested on single ring events, the ring size and shape is faithfully reproduced. When generalized to multiring events, this feature may allow assignment of PMT hits to the appropriate rings which might then be used to reconstruct multiple particle tracks.

4. In a more speculative direction, work is in progress on the application of neutral networks to recognition of the pattern of PMT hits in an event.

All of this work is in early stages of development. Nevertheless, sufficient progress has been made which encourages us to believe that one or more of these algorithms will be successful.

Summary

In this chapter we have discussed the methods of data reduction and analysis inherited from previous collaborations on imaging water Cherenkov detectors, and described in some detail how they are directly applied to the data of E889 principally by computer processing. Specifically, we have confronted the questions of muon-electron recognition and separation, vital to a search in the $\nu_\mu \leftrightarrow \nu_e$ oscillation channel; and of the efficiency with which WNC(π^0) events can be recognized and detected, essential to accurate measurement of the ratio WCC($QE\mu$)/WNC(π^0) within each of the four E889 detectors. Aberrant WNC(π^0) events may simulate quasielastic electron events and WCC(π^0) may simulate WNC(π^0) events if the muon is not evident. Both of these sources of background may be largely eliminated in direct ways, as described in this chapter, so that they are unlikely to introduce serious limitation

of the sensitivity of E889 oscillation searches. A more detailed analysis of the effect of these backgrounds on the E889 sensitivity is given in Chapter V. Finally, a brief progress report was given on methods of automatic pattern recognition and reconstruction of multiring events under development by the E889 collaboration.

Table 1: Result of visual identification of WCC(π^0) and WNC(π^0) events from Cherenkov ring patterns. Entries marked with an asterisk do not show a ring with a clear sharp outer edge.

Classification	WNC(π^0)	WCC(μ not seen)	WCC(μ seen)
1 ring	18.1%	1.5%	0.5%
1 ring +	20.8	1.5	2.9
2 rings	54.2	6.1	11.2
2 rings +	3.8	4.1*	18.8
3 rings	1.9	4.7*	41.8
3 rings +	0.4	1.0*	5.6
unidentifiable	0.8	0.3	0.0

Table 2: Result of visual identification of WNCπ^0 events for three PMT coverages.

Classification	5.4% coverage	10.3% coverage	18.6% coverage
1 ring	59%	29%	34%
2 rings	40	66	60
3 rings	0	4	1
$>$ 3 rings	1	0	5
unidentifiable	0	1	0

References

The publications in refereed journals of the Kamiokande & IMB groups, following the usual custom, tend to emphasize physical results rather than methods and techniques. The latter are, however, described in detail in the Ph.D. theses, Master's thesis and undergraduate senior theses, which are listed below.

1. K. Arisaka, "Experimental Search for Nucleon Decay", Ph.D. Thesis, University of Tokyo (1984) unpublished.

2. T. Kajita, "Search for Nucleon Decays in Antineutrino Plus Mesons", Ph.D. thesis, University of Tokyo (1985) unpublished.

3. S.C. Seidel, "A Search for Nucleon Decay Employing Particle Identification, Invariant Masses, and Complete Track Reconstruction in a Water Cherenkov Detector", Ph.D. Thesis, University of Michigan (1987) unpublished.

4. M. Nakahata, "Search for ^8B Solar Neutrinos at Kamiokande II", P.H.D. Thesis, University of Tokyo (1988) unpublished.

5. W. Zhang, "Experimental Search for Electron Antineutrinos from Past Supernovae", Ph.D. Thesis, University of Pennsylvania (1988) unpublished.

6. M. Takita, "An Experimental Study of the Atmospheric Neutrino Flux with the Kamiokande Detector", Ph.D. Thesis, University of Tokyo (1989) unpublished.

7. S.B. Kim, "Real time, Directional Measurement of ^8B Solar Neutrinos in the Kamiokande-II Detector and Search for Short-Time Variation", Ph.D. Thesis, University of Pennsylvania (1989) unpublished.

8. D.W. Casper, "Experimental Neutrino Physics and Astrophysics with the IMB-3 Detector", Ph.D. Thesis, University of Michigan (1990) unpublished.

9. E.D. Frank, "A Study of Atmospheric Neutrino Interactions in the Kamiokande-II Detector", Ph.D. Thesis, University of Pennsylvania (1992) unpublished.

10. Scott Smith, "Prospects for the Observation of Low Energy Neutrinos in a Massive Imaging Water Cherenkov Detector", M.S. Thesis, University of Pennsylvania (1985) unpublished.

11. Jared Anderson, "Computer Simulation of a Long Baseline Neutrino Oscillation Experiment", Undergraduate Thesis, University of Pennsylvania (1994) unpublished.

12. Siun-Chuon Mau, "Reconstruction Program for a Long Baseline Neutrino Oscillation Experiment", Senior Thesis, University of Pennsylvania (1994) unpublished.

Figure Captions

Fig. 1. (a) Vertex resolution for muons (open circles) and electrons (solid circles) as a function of the total number of photoelectrons (and momentum). (b) Angular resolution for muons and electrons as a function of total number of photoelectrons. From the Ph.D. thesis of M. Takita.

Fig. 2. Preliminary results of muon-electron separation from the Kamiokande-KEK test detector. (a) Data. (b) Monte Carlo simulation.

Fig. 3. Simulated WNC(π^0) event showing the two Cherenkov rings from the decay $\pi^0 \to \gamma\gamma$.

Fig. 4. Simulated WCC(π^0) event showing the two fuzzy edged rings from the π^0 decay and the sharp edged ring from the muon.

Fig. 5. Reconstruction of the invariant π^0 mass from a number of simulated WNC(π^0) decays as in Fig. 2 from the Ph.D. thesis of K. Arisaka.

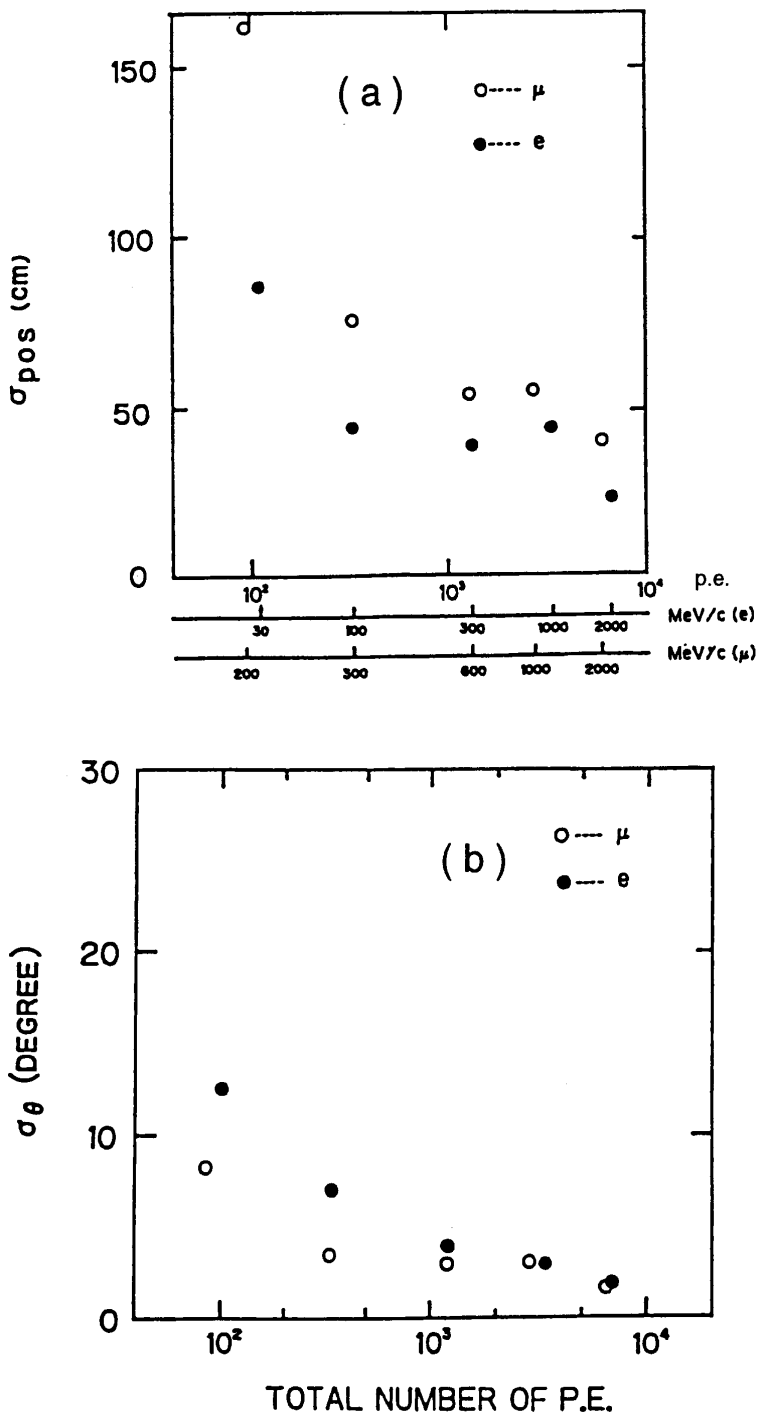
(a)
μ
e
150
100
50
0
σ_{pos} (cm)
10^2
10^3
10^4
p.e.
30
100
300
1000
2000
MeV/c (e)
200
300
600
1000
2000
MeV/c (μ)
(b)
μ
e
30
20
10
0
σ_θ (DEGREE)
10^2
10^3
10^4
TOTAL NUMBER OF P.E.

Fig. 1

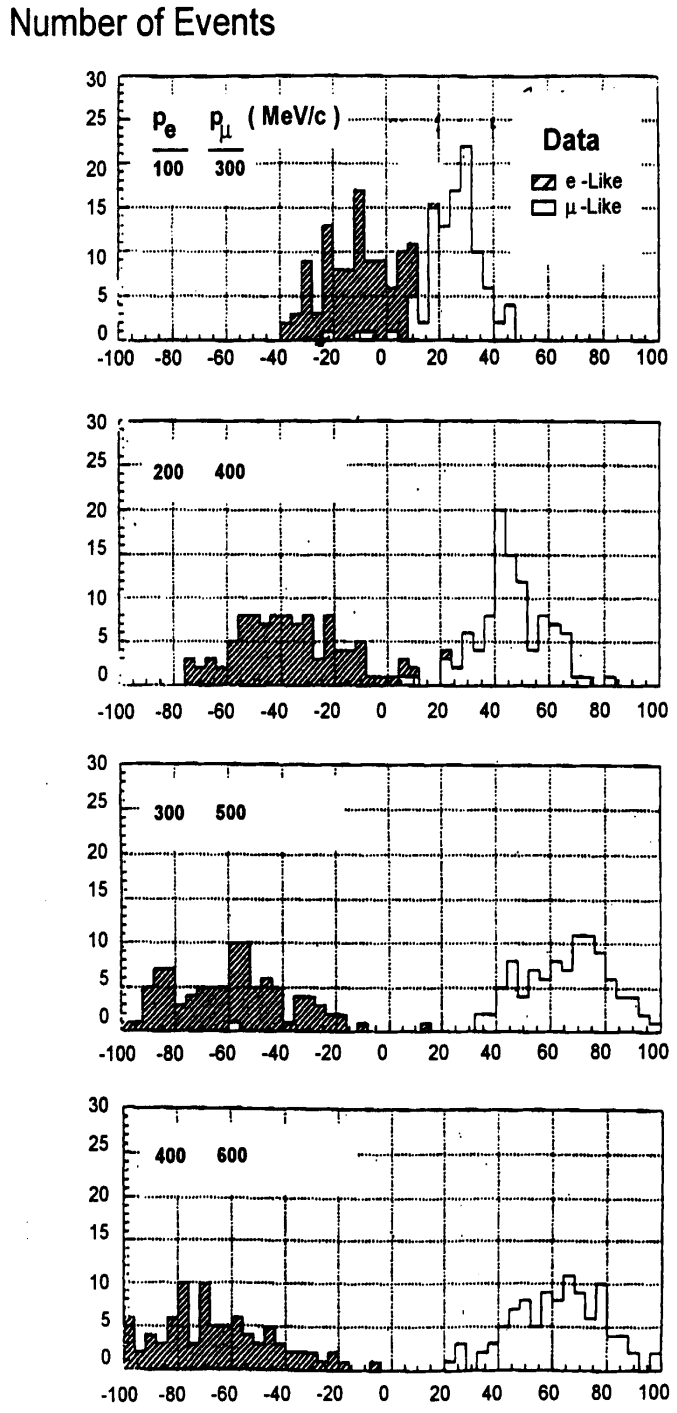
Number of Events
p_e / 100
p_μ / 300 (MeV/c)
Data
e -Like
μ -Like
200 400
300 500
400 600
$\log_{10} L(\mu) - \log_{10} L(e)$

Fig. 2a

Fig. 2a

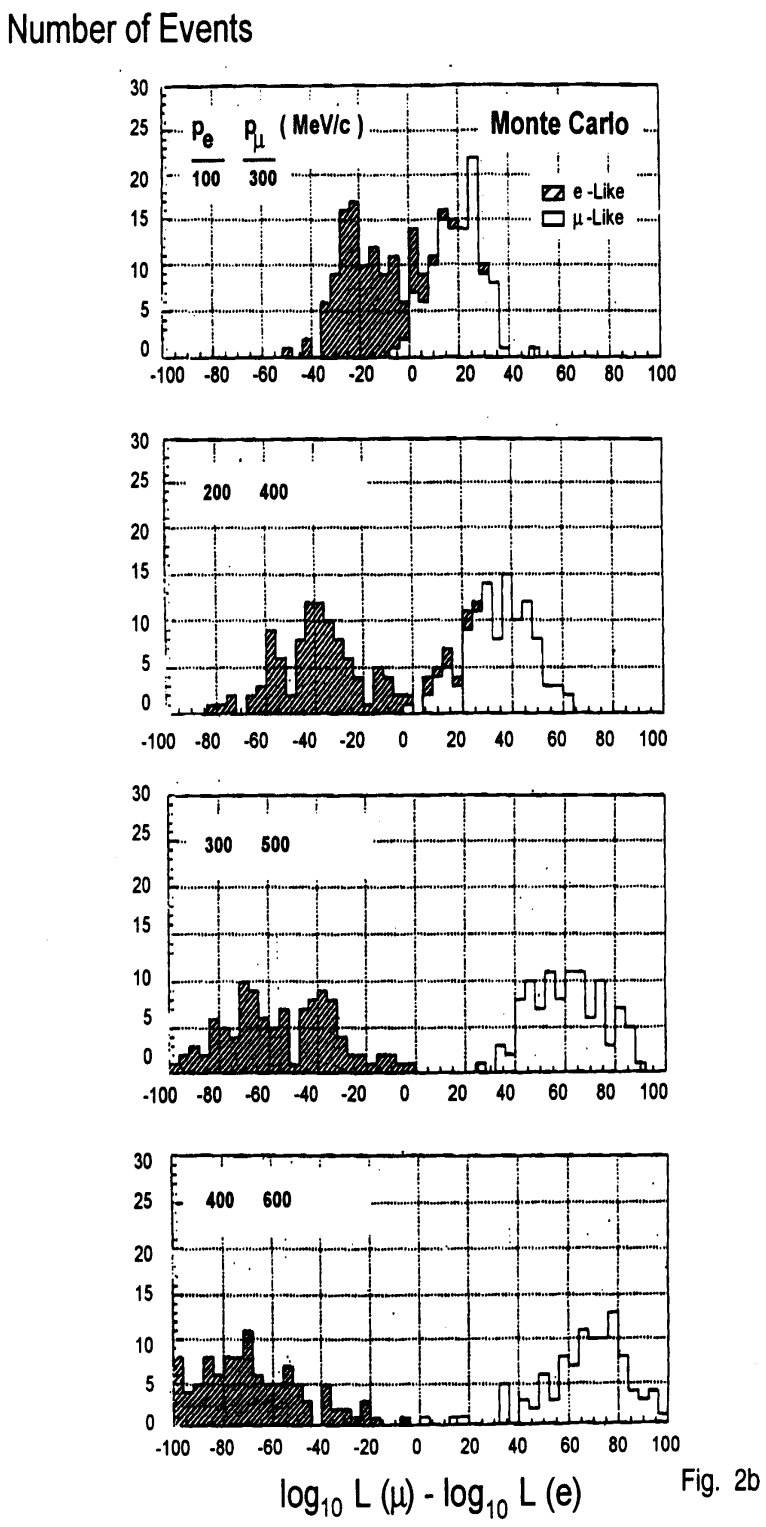
Number of Events
p_e p_μ (MeV/c)
100 300
Monte Carlo
e -Like
μ -Like
200 400
300 500
400 600
$\log_{10} L(\mu) - \log_{10} L(e)$

Fig. 2b

Fig. 2b

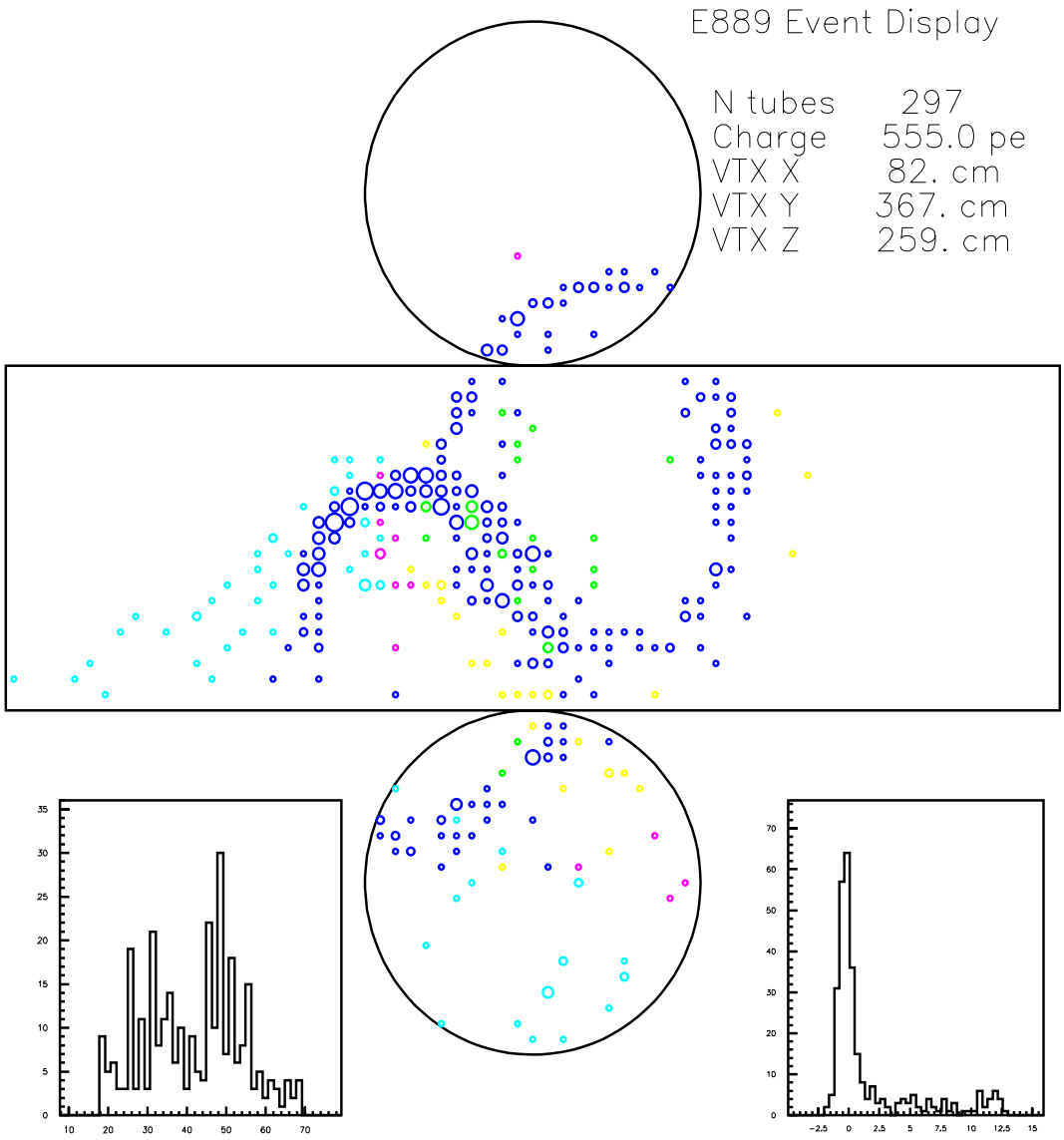
E889 Event Display
N tubes 297
Charge 555.0 pe
VTX X 82. cm
VTX Y 367. cm
VTX Z 259. cm

Fig. 3

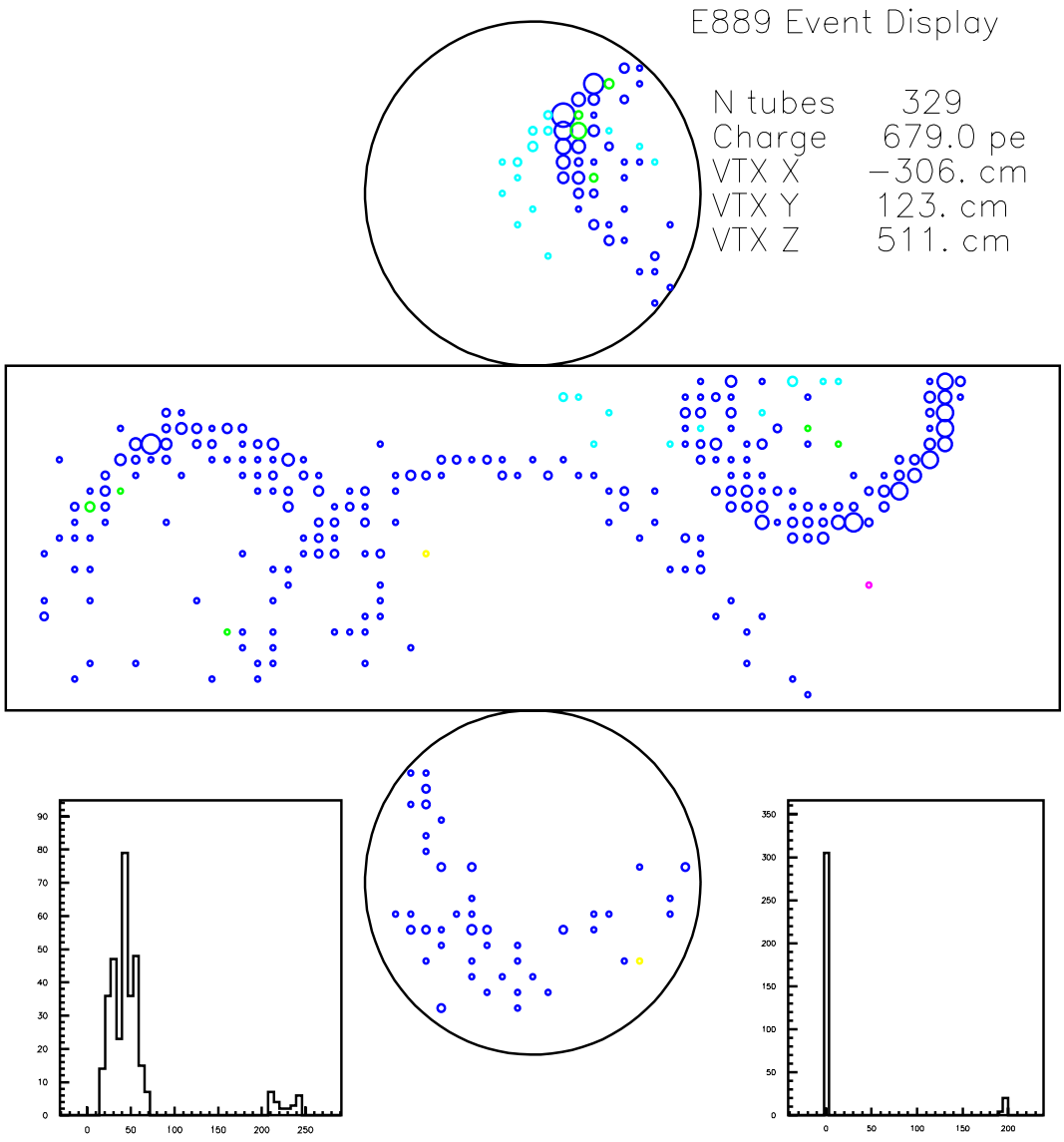
E889 Event Display
N tubes 329
Charge 679.0 pe
VTX X −306. cm
VTX Y 123. cm
VTX Z 511. cm

Fig. 4

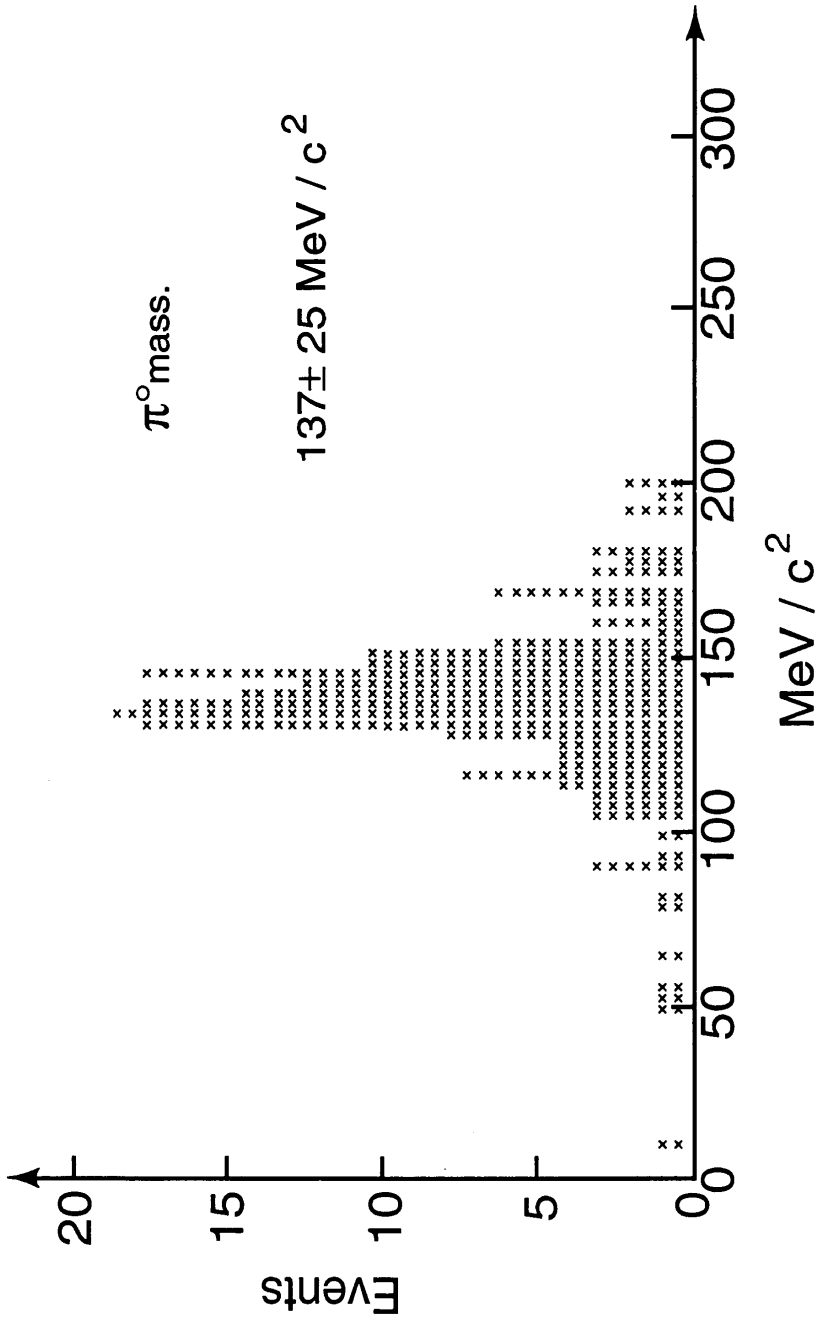
π°mass.
137± 25 MeV / c^2
Events
MeV / c^2
0
5
10
15
20
50
100
150
200
250
300

Fig. 5